Electronic Supplementary Material (ESI) for ChemComm.

Supporting Information for

Arrested α-Hydride Migration Activates a Phosphido Ligand for C-H Insertion

Anne K. Hickey, Salvador B. Muñoz, III, Sean A. Lutz, Maren Pink, Chun-Hsing Chen and Jeremy M. Smith

Contents

Experimental

General Considerations. All manipulations were performed under a nitrogen atmosphere by standard Schlenk techniques or in an MBraun glove box. Glassware was dried at 130 °C overnight before cooling under a dynamic vacuum in an antechamber. Manipulations involving high vacuum and inert or reactive gases were performed using standard Schlenk techniques in double-manifold glass lines. Diethyl ether (Et_2O), tetrahydrofuran (THF), toluene, and pentane were purified by a Glass Contour solvent purification system. Celite was dried overnight at 130 °C under vacuum. The compounds $PhB(MesIm)_3FeCl$,[1] $PhB(^tBuIm)_3FeCl$,[2] 3,5-dicyclohexylimidazole (Cy_2Im),[3] and $LiPH(C_6H_5)(THF)$,[4] prepared by literature methods. Benzene-d_6 (C_6D_6, Cambridge Isotope Laboratories, CIL) was degassed by three consecutive freeze-pump-thaw cycles on a Schlenk line and then placed over sodium and molecular sieves for 12 h prior to use. ^1H NMR spectroscopic data were recorded on Varian spectrometers. Solution magnetic susceptibilities were determined by Evans' method.[5] IR spectra were recorded with a Perkin Elmer spectrophotometer. UV-Vis spectroscopic data were collected on an Agilent Technologies Cary 60 UV-Vis instrument, with a Unisoku Scientific Instruments cryostat for variable-temperature experiments. Elemental analysis was conducted by Midwest Microlab, LLC (Indianapolis, IN). Mass spectrometry measurements were made using an Agilent 1200 HPLC-6130 MSD spectrometer. Mössbauer spectra were recorded on a SEE Co spectrometer. The sample temperature was controlled using a SVT-400 Dewar from Janis equipped with a Lake Shore 255 Temperature Controller. The isomer shifts are reported relative to the centroid of the spectrum of α-Fe at 298 K. Samples were prepared by grinding spectroscopically pure material into a fine powder and then mounting in a cup, plugged with a fitted O-ring sealed cap. Data

analysis was performed using the program WMOSS[6] and quadrupole doublets were fitted to Lorentzian lineshapes.

PhB(^{t}BuIm)$_3$Fe(PH(C_6H_5)) (1a). A vial was charged with PhB(^{t}BuIm)$_3$FeCl (211 mg, 0.38 mmol), and LiPH(C_6H_5) (80 mg, 0.40 mmol), and C_6H_6 (10 mL). The slurry turned red-brown and was stirred overnight, filtered through Celite, and taken to dryness, leaving a brown-red powder (186 mg,78% yield). Crystals suitable for X-ray diffraction were grown from a concentrated pentane-ether solution of the complex left at room temperature overnight. ^{1}H NMR (400 MHz, C_6D_6, 25 ^{o}C) δ 68 (3H, Im-*H*); 46 (3H, Im-*H*); 33 (2H, *m*/*o*-B(C_6H_5)); 26 (2H, P(C_6H_5)); 23 (2H, P(C_6H_5)); 15 (2H, *m*/*o*-B(C_6H_5)); 13 (1H, *p*-B(C_6H_5)); -11 (27H, ^{t}Bu); -12 (1H, P(C_6H_5)). IR (KBr) ν_{PH} = 2299 cm^{-1}. μ_{eff} = 4.0(2) μ_B (Evans method, 25 °C, C_6D_6). Analysis cald for $C_{33}H_{44}BFeN_6P$: C 63.68, H 7.13, N 13.50. Found C 63.44, H 7.17, N 13.43.

[PhB(Cy_2Im)$_3$][OTf]$_2$. A Schlenk flask was charged with Cy_2Im (1.36 g, 5.9 mmol), $PhBCl_2$ (0.32 g, 2.0 mmol), and 40 mL toluene. TMSOTf (0.87g, 3.9 mmol) was added dropwise, giving a white slurry. The slurry was refluxed overnight. The toluene was evaporated under vacuum. The remaining oil was extracted into cold ether. The resulting white powder was recovered on a filter frit and dried under vacuum, giving [PhB(CyIm)$_3$][OTf]$_2$ (1.596 g, 69% yield). ^{1}H NMR (400 MHz, $CDCl_3$, 25 °C): δ 8.45 (s, 3H, Im-*H*), 7.43 (s, 3H, B(C_6H_5)), 7.18 (*d*, J_{HH} = 8 Hz, 2H, B(C_6H_5)), 6.79 (s, 3H, Im-*H*), 3.98 (pseudo-*t*, J_{HH} = 12 Hz, 3H, Cy-*H*), 2.59 (pseudo-*t*, J_{HH} = 12 Hz, 3H, Cy-*H*), 2.14-1.20 (m, 60H, Cy-*H*). ES-MS: Found 933.5 [(PhB(Cy_2Im)$_3$)(SO_3CF_3)]$^+$; $C_{52}H_{77}BF_3N_6O_3S$ requires 933.6.

PhB(Cy_2Im)$_3$FeCl. A vial was charged with [PhB(Cy_2Im)$_3$][OTf]$_2$ (296 mg, 0.27 mmol) and 10 mL of ether. The slurry was chilled to -35 °C. *n*-BuLi (0.51 mL, 1.6 M in hexanes) was added, and the slurry was stirred for 2 hours, gradually turning more clear and colored yellow.

$FeCl_2(THF)_{1.5}$ (70 mg, 0.30 mmol) was added as a solid. The tan slurry was stirred overnight, taken to dryness, extracted into toluene, and filtered through Celite. The toluene was evaporated under vacuum, leaving $PhB(Cy_2Im)_3FeCl$ as a tan solid (177 mg, 75% yield). Crystals suitable for X-ray diffraction were grown from a pentane solution stored at -35 °C for 2 days. ^1H NMR (400 MHz, C_6D_6, 25 °C): δ 62 (3H, Im-*H*), 43 (2H, $B(C_6H_5)$), 22 (2H, $B(C_6H_5)$), 19 (1H, $B(C_6H_5)$), 6 (6H, Cy-*H*)), 4 (6H, Cy-*H*), 3.7 (3H, Cy-*H*), 3 (6H, Cy-*H*), 1.5 (6H, Cy-*H*), 1.1 (6H, Cy-*H*), 0.6 (6H, Cy-*H*), 0.5 (3H, Cy-H), 0 (3H, Cy-H), -0.2 (3H, Cy-*H*), -3 (6H, Cy-*H*), -4 (6H, Cy- *H*), -45 (6H, Cy- *H*). μ_{eff} (Evans', THF-d_8, 25 °C): 5.0(1) μ_B. Analysis cald for $C_{51}H_{74}BClFeN_6$: C 70.14, H 8.54, N 9.62. Found C 69.89, H 8.66, N 9.24.

$PhB(Cy_2Im)_3Fe(PH(C_6H_5))$ (1b). A vial was charged with $PhB(Cy_2Im)_3FeCl$ (56 mg, 0.064 mmol), $LiPH(C_6H_5)$ (15 mg, 0.075 mmol), and 10 mL of ether. The slurry was stirred overnight. The solvent was evaporated, and the remaining powder extracted into pentane and filtered through Celite. The solution was dried under vacuum, leaving $PhB(Cy_2Im)_3Fe(PH(C_6H_5))$ as a red-brown powder (48 mg, 79 % yield). Crystals suitable for X-ray diffraction were grown from a pentane solution stored at -35 °C for 2 days. ^1H NMR (400 MHz, C_6D_6, 25 °C): δ 45 (3H, Im-*H*), 25 (3H, Im-*H*), 22 (2H, $B(C_6H_5)$), 13 (2H, $B(C_6H_5)$), 12 (1H, $B(C_6H_5)$), 5 (6H, Cy- *H*), 2 (12H, Cy-*H*), 1.2 (12H, Cy- *H*), 0.9 (12H,Cy- *H*), -0.5 (12H, Cy- *H*), -0.7 (6H, Cy- *H*),-12 (3H, Cy- *H*), -20 (3H, Cy- *H)*. μ_{eff} (Evans', C_6D_6, 25 °C): 4.6(2) μ_B. IR (KBr pellet) ν_{PH} 2255 cm^{-1}. Analysis cald for $C_{57}H_{80}BFeN_6P$: C 72.30, H 8.61, N 8.88. Found C 72.05, H 8.61, N 8.68.

Spectroscopic characterization of $PhB(MesIm)_3Fe(PH(C_6H_5))$ (1c). A J. Young NMR tube was charged with $PhB(MesIm)_3FeCl$ (25 mg, 0.03 mmol) and $LiPH(C_6H_5)$ (7 mg, 0.04 mmol), and C_6D_6 (0.5 mL). The slurry immediately turned purple. After 20 min, quantitative conversion to $PhB(MesIm)_3Fe(PH(C_6H_5))$ was observed by ^1H NMR spectroscopy. Due to the thermal

instability of this complex, an isolated yield could not be obtained. ^{1}H NMR (400 MHz, C_6D_6, 25 ^{o}C) δ 67 (3H, Im-*H*); 57 (3H, Im-*H*); 37 (2H, P(C_6H_5)); 31 (2H, P(C_6H_5)); 17 (2H, *m*-B(C_6H_5)); 15 (1H, *p*-B(C_6H_5)); 3(6H, Mes *m*-H); -22 (18H, Mes *o*-CH_3), -24 (1H, P(C_6H_5)).

Complex 2. A vial was charged with PhB(MesIm)$_3$FeCl (43 mg, 0.058 mmol), LiPH(C_6H_5) (18 mg, 0.094 mmol), and C_6D_6 (2 mL). The slurry initially turns purple, then turns brown over hours. After stirring 16 h, the slurry was filtered and an aliquot was transferred into a J. Young tube. The yield was observed to be quantitative by ^{1}H NMR spectroscopy. Work up of the slurry by filtering and drying usually results in a mixture of complexes **2** and **3**. Crystals suitable for X-ray diffraction were grown from a concentrated pentane solution stored at -35 ^{o}C overnight. ^{1}H NMR (500 MHz, C_6D_6, 25 ^{o}C): δ 8.35 (*d*, 2H, *J* = 4 Hz); 7.67 (*d*, 1H, *J* = 2 Hz); 7.50 (*t*, 2H, *J* = 8Hz); 7.43 (*t*, 1H, *J* = 4 Hz); 7.24 (*d*, 1H, *J* = 1.5 Hz); 6.98 (*d*, 4H, *J* = 1.5 Hz); 6.83 (*s*, 2H); 6.73 (*s*, 1H); 6.69 (*s*, 1H); 6.58 (*s*, 1H); 6.36 (*d*, 1H, *J* = 1 Hz); 6.34 (*d*, 1H, *J* = 1 Hz); 6.30 (*d*, 1H, *J* = 1 Hz); 5.96 (*s*, 1H); 5.76 (*d*, 1H, $^{1}J_{HP}$ = 285 Hz, P*H*); 2.91 (pseudo *t*, 1H, *J* = 15 Hz, PCH_2); 2.75 (*d*, 1H, *J* = 8 Hz, PCH_2); 2.21 (*s*, 3H, Mes-CH_3); 2.10 (*s*, 3H, Mes-CH_3); 2.08 (*s*, 3H, Mes-CH_3); 2.05(*s*, 3H, Mes-CH_3); 2.03 (*s*, 3H, Mes-CH_3); 2.02 (*s*, 3H, Mes-CH_3); 1.97 (*s*, 3H, Mes-CH_3); 1.87 (*s*, 3H, Mes-CH_3); -10.68 (*d*, 1H, $^{2}J_{HP}$ = 55 Hz). ^{31}P{^{1}H} NMR (162 MHz, C_6D_6, 25 ^{o}C) δ 69.7. ^{31}P NMR (162 MHz, C_6D_6, 25 °C) δ 69.7 (*dd*, $^{1}J_{HP}$ = 281 Hz, $^{2}J_{HP}$ =57 Hz). IR (C_6H_6) ν_{NN} = 2105 cm^{-1}, ν_{PH} = 2305 cm^{-1}. Analysis Cald. for $C_{48}H_{50}BFeN_8P$: C 68.91, H 6.02, N 13.39. The thermal instability of this complex prevents us from obtaining elemental analysis data.

Spectroscopic characterization of complex 2-*d*. A J. Young tube was charged with PhB(MesIm)$_3$FeCl (20 mg, 0.027 mmol), LiPD(C_6H_5) (11 mg, 0.094 mmol), and C_6D_6 (0.5 mL). The slurry initially turns purple, then turns brown over hours. The yield was observed to be quantitative by ^{1}H NMR spectroscopy. ^{1}H NMR (400 MHz, C_6D_6, 25 ^{o}C): δ 8.35 (*d*, 2H, *J* = 4

Hz); 7.68 (*d*, 1H, *J* = 2 Hz); 7.51 (*t*, 2H, *J* = 8Hz); 7.44 (*t*, 1H, *J* = 4 Hz); 7.25 (*d*, 1H, *J* = 1.5 Hz); 6.98 (*d*, 4H, *J* = 1.5 Hz); 6.83 (*s*, 2H); 6.73 (*s*, 1H); 6.69 (*s*, 1H); 6.58 (*s*, 1H); 6.36 (*d*, 1H, *J* = 1 Hz); 6.33 (*d*, 1H, *J* = 1 Hz); 6.30 (*d*, 1H, *J* = 1 Hz); 5.97 (*s*, 1H); 5.76 (*d*, 1H, $^1J_{HP}$ = 285 Hz, P*H*); 2.91 (pseudo *t*, 1H, *J* = 15 Hz, PCH_2); 2.76 (*d*, 1H, *J* = 8 Hz, PCH_2); 2.21 (*s*, 3H, Mes-CH_3); 2.10 (*s*, 3H, Mes-CH_3); 2.08 (*s*, 3H, Mes-CH_3); 2.05(*s*, 3H, Mes-CH_3); 2.03 (*s*, 3H, Mes-CH_3); 2.02 (*s*, 3H, Mes-CH_3); 1.97 (*s*, 3H, Mes-CH_3); 1.87 (*s*, 3H, Mes-CH_3). ^{2}H NMR (61.4 MHz, C_6D_6, 25 ^{o}C) δ -9.13 ppm (s). $^{31}P\{^1H\}$ NMR (162 MHz, C_6D_6, 25 ^{o}C) δ 69.7.

Complex 3. A vial was charged with PhB(MesIm)$_3$FeCl (70 mg, 0.095 mmol), LiPH(C_6H_5) (19 mg, 0.012 mmol), and C_6H_6 (2 mL). The slurry was stirred overnight, taken to dryness, extracted into pentane, filtered through Celite, and dried under vacuum. The brown powder was washed with pentane and dried, giving PhB(MesIm)Fe(CH_2)(N_2)(PH(C_6H_5)) as a golden yellow powder (45 mg, 58% yield). ^{1}H NMR (500 MHz, C_6D_6, 25 ^{o}C): δ 8.31 (*d*, 2H, *J* = 6 Hz); 7.73 (*d*, 1H, *J* = 2 Hz); 7.52 (*t*, 2H, *J* = 8Hz); 7.46 (*d*, 1H, *J* = 5 Hz); 7.43 (*d*, 1H, *J* = 1 Hz); 6.98 (*d*, 1H, *J* = 1.5 Hz); 6.81 (*s*, 1H); 6.79 (*s*, 1H); 6.76 (*s*, 1H); 6.74 (*s*, 1H); 6.67 (*d*, 1H, *J* = 1.5 Hz); 6.40 (*s*, 1H); 6.34 (*d*, 1H, *J* = 2 Hz); 6.25 (*d*, 1H, *J* = 2 Hz); 6.21 (*s*, 1H); 5.95 (*s*, 1H); 4.73 (*d*, 1H, $^1J_{HP}$ = 320 Hz); 2.80 (pseudo *t*, 1H, *J* = 10 Hz, PCH_2); 2.49 (*t*, 1H, *J* = 15 Hz, PCH_2); 2.26 (*s*, 3H, Mes-CH_3); 2.16 (*s*, 3H, Mes-CH_3); 2.13 (*s*, 3H, Mes-CH_3); 2.02 (*s*, 3H, Mes-CH_3); 1.97 (*s*, 3H, Mes-CH_3); 1.92 (*s*, 3H, Mes-CH_3); 1.71 (*s*, 3H, Mes-CH_3); 1.87(*s*, 3H, Mes-CH_3); 0.91 (*d*, 1H, *J* = 10 Hz); 0.87 (*t*, 1H, *J* = 10 Hz). $^{31}P\{^1H\}$ NMR (162 MHz, C_6D_6, 25 ^{o}C) δ 56.9. ^{31}P NMR (162 MHz, C_6D_6, 25 ^{o}C) δ 56.9 (*d*, $^1J_{HP}$ = 322 Hz). IR (C_6H_6) ν_{NN} = 2095 cm^{-1}, ν_{PH} = 2312cm^{-1}. ESI-MS: Found 806.3 {M$^+$}; $C_{48}H_{48}BFeN_6P$ requires 806.58. Found 835.3 {M+H}$^+$; $C_{48}H_{48}BFeN_8P$ requires 834.32. Analysis cald for $C_{48}H_{48}BFeN_6P$: C 69.08, H 5.80, N 13.43. Found C 68.78, H 5.80, N 13.12.

Supplementary Figures

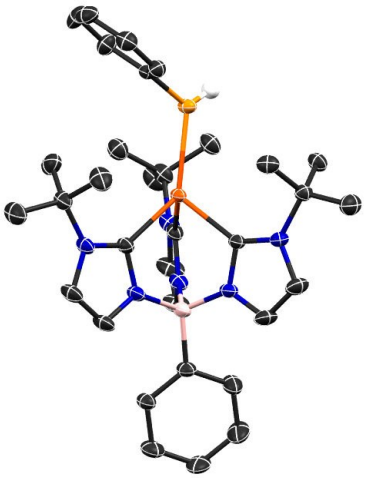

Figure S1. Molecular structure of complex **1a**. Most H atoms are omitted for clarity.

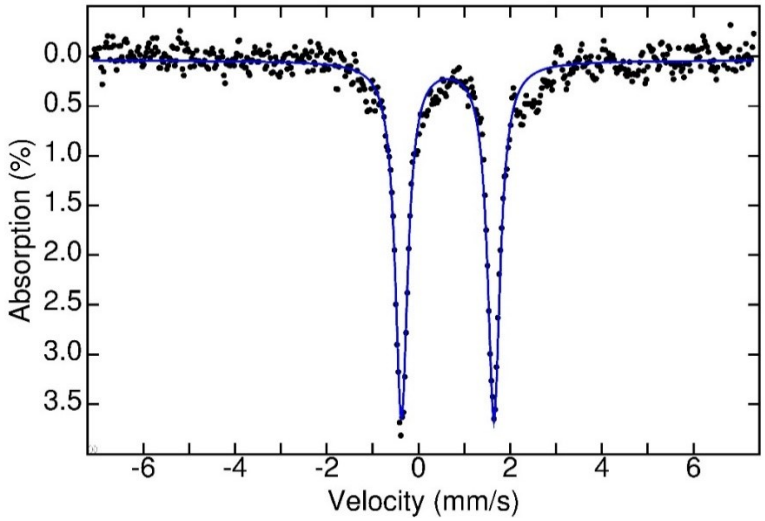

Figure S2. Mössbauer spectrum of PhB(^{t}BuIm)$_3$FeCl at zero applied field. Parameters: δ 0.64 mm/s, ΔE_Q 2.02 mm/s, Γ = 0.33 mm/s. These spectral parameters are similar to those of other iron(II) tris(carbene)borate complexes.[7]

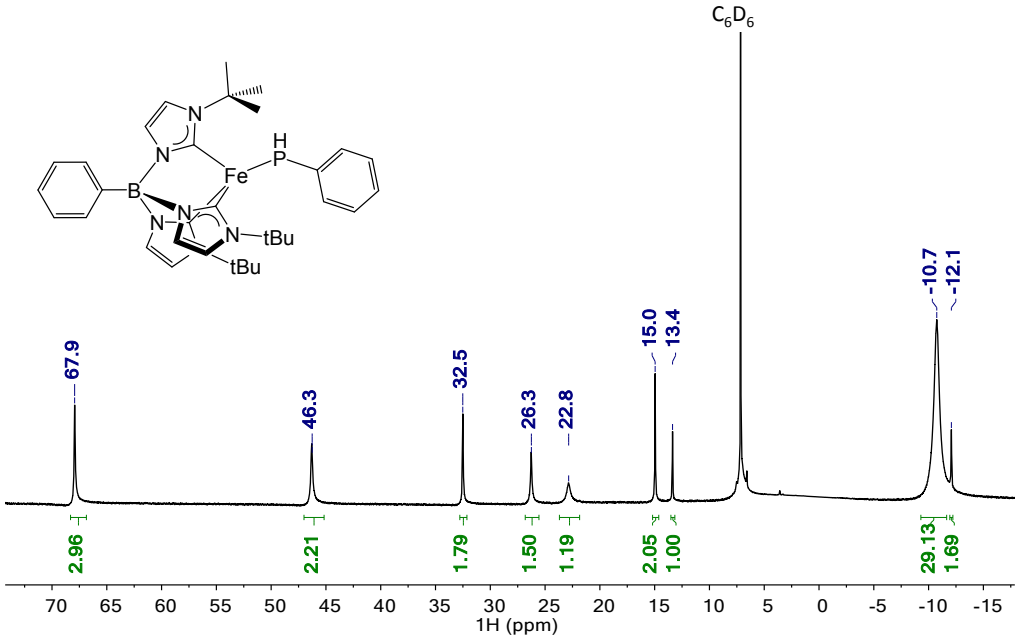

Figure S3. ^{1}H NMR spectrum (500 MHz, C_6D_6, 25 °C) of complex PhB(^{t}BuIm)$_3$ Fe(PH(C_6H_5))(**1a**).

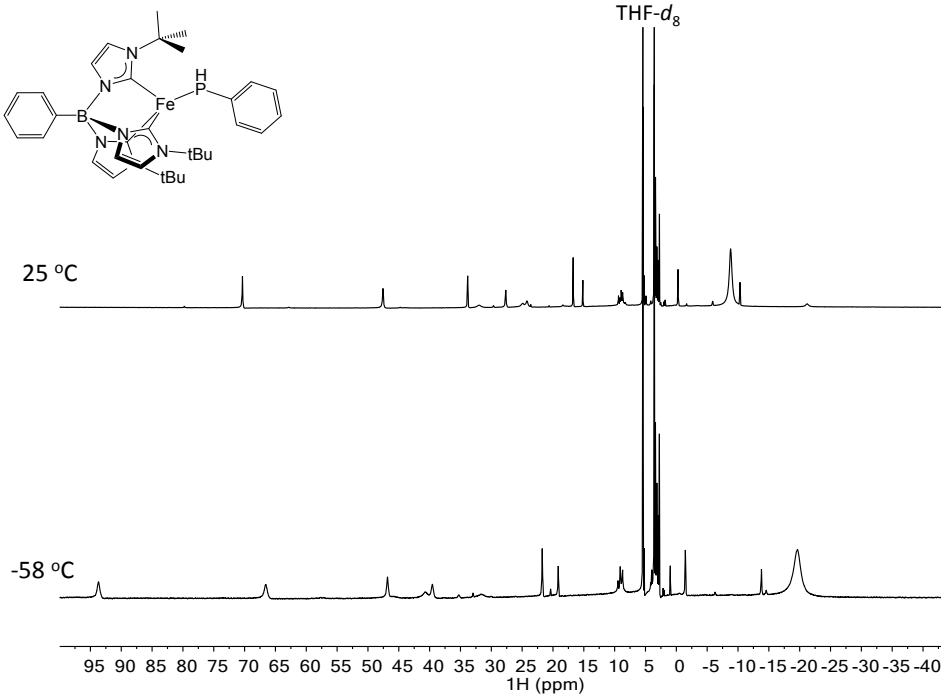

Figure S4. Variable temperature ^{1}H NMR spectra (400 MHz, C_6D_6, 25 °C) of complex PhB(^{t}BuIm)$_3$ Fe(PH(C_6H_5))(**1a**) at 25 °C (top) and -58 °C (bottom).

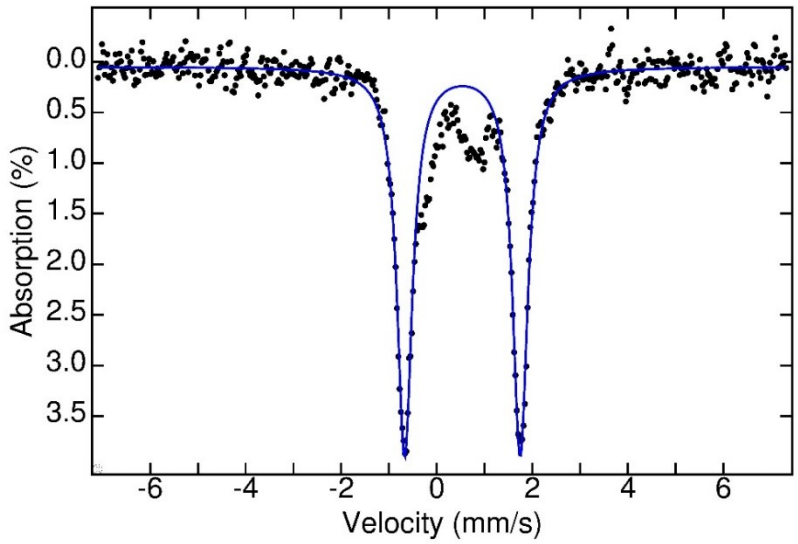

Figure S5. Mössbauer spectrum of complex PhB(^{t}BuIm)$_3$Fe(PH(C_6H_5)) (**1a**) at zero applied field (purple). Parameters for **1a**: δ 0.54 mm/s, ΔE_Q 2.42 mm/s, Γ = 0.39 mm/s. These spectral parameters for **1a** are similar to those of other iron(II) tris(carbene)borate complexes.[7]

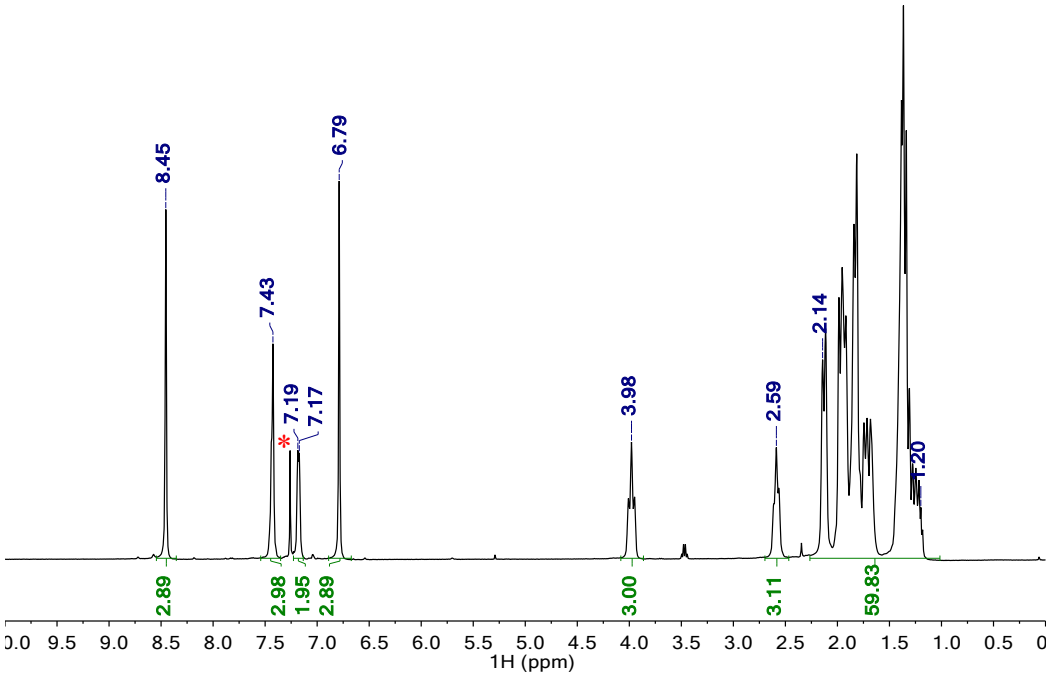

Figure S6. ^{1}H NMR spectrum (400 MHz, $CDCl_3$, 25 °C) of $[Ph(Cy_2Im)_3][SO_3CF_3]_2$. The (*) shows $CDCl_3$.

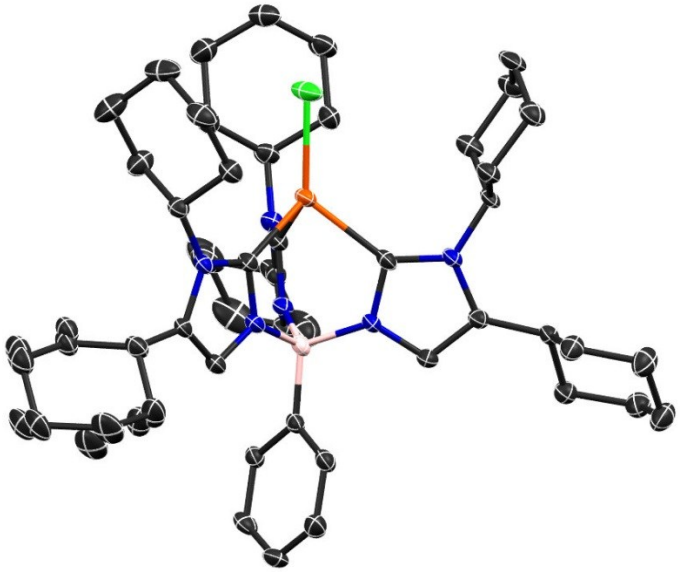

Figure S7. Molecular structure of $PhB(Cy_2Im)_3FeCl$. One co-crystallized ether molecule and H atoms are omitted for clarity.

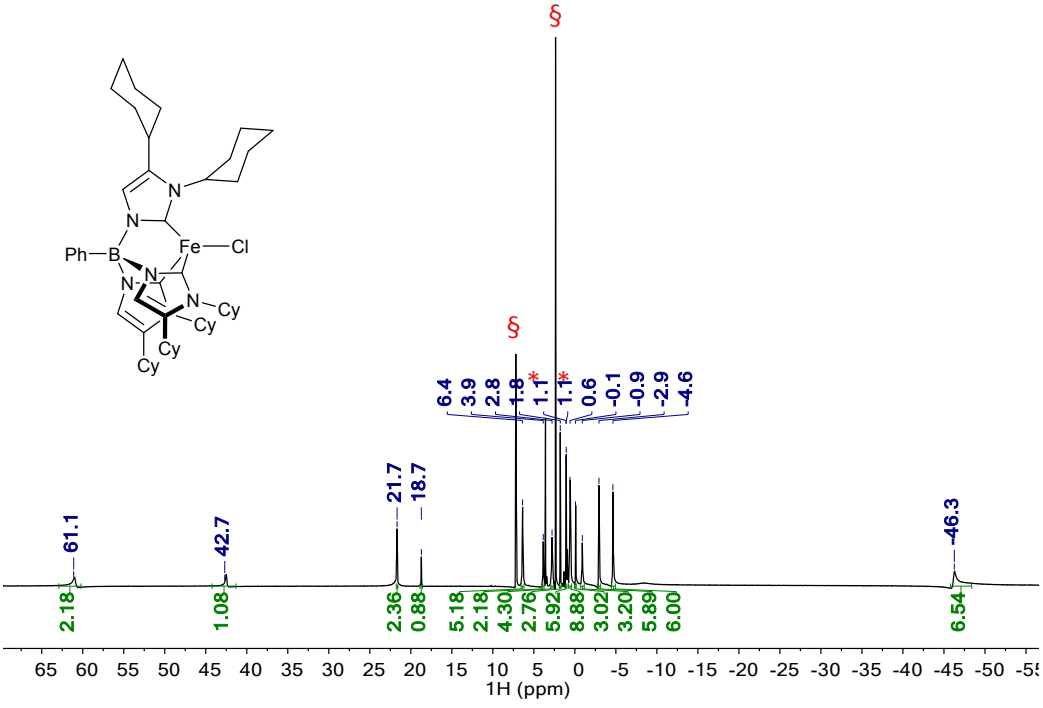

Figure S8. ^{1}H NMR spectrum (400 MHz, THF-d_8, 25 °C) of Ph(Cy$_2$Im)$_3$FeCl. The (*) shows THF-d_8, and the (§) shows residual toluene.

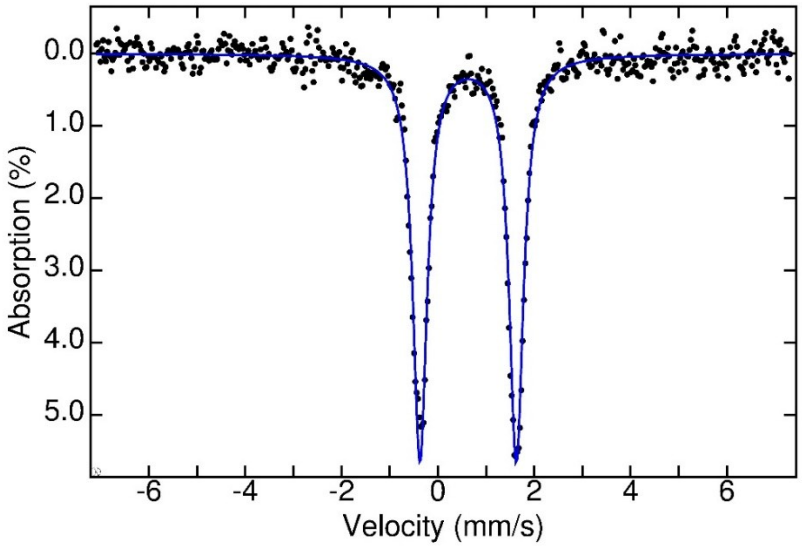

Figure S9. Mossbauer spectrum of complex PhB(Cy$_2$Im)$_3$FeCl. Parameters: δ 0.63 mm/s, ΔE_Q 2.00 mm/s, Γ = 0.36 mm/s. These spectral parameters are similar to those of other iron(II) tris(carbene)borate complexes.[7]

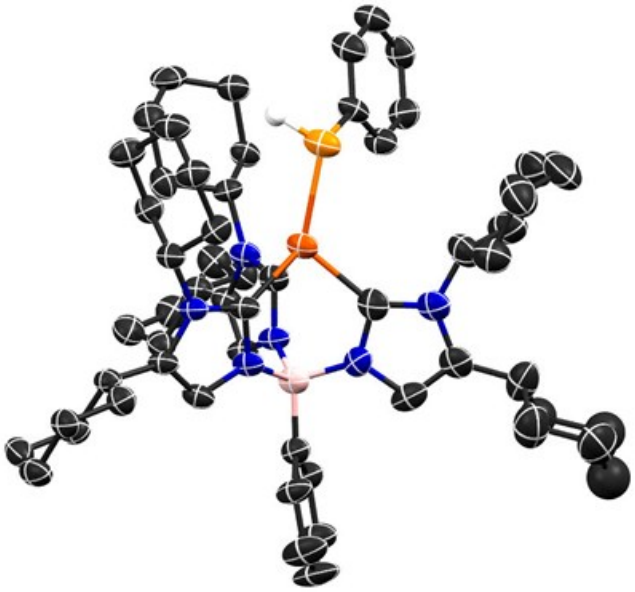

Figure S10. Molecular structure of complex **1b**. One co-crystallized pentane molecule and most H atoms are omitted for clarity.

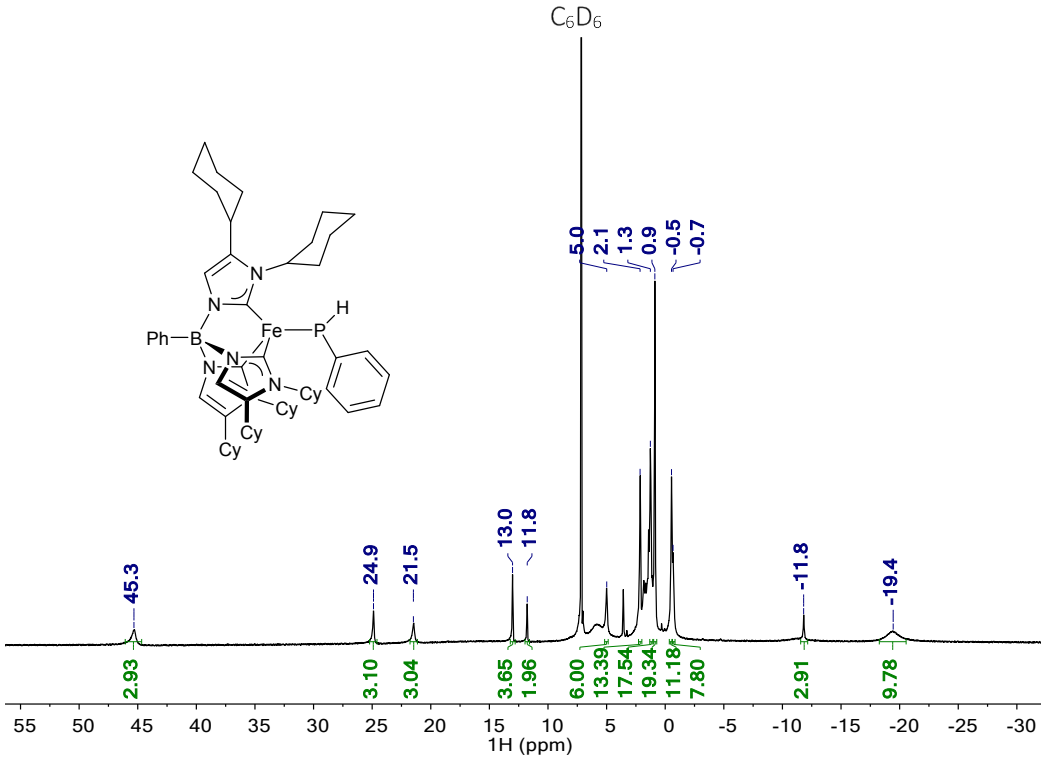

Figure S11. ^{1}H NMR spectrum (400 MHz, C_6D_6, 25 °C) of $Ph(Cy_2Im)_3FePHPh$ (**1b**).

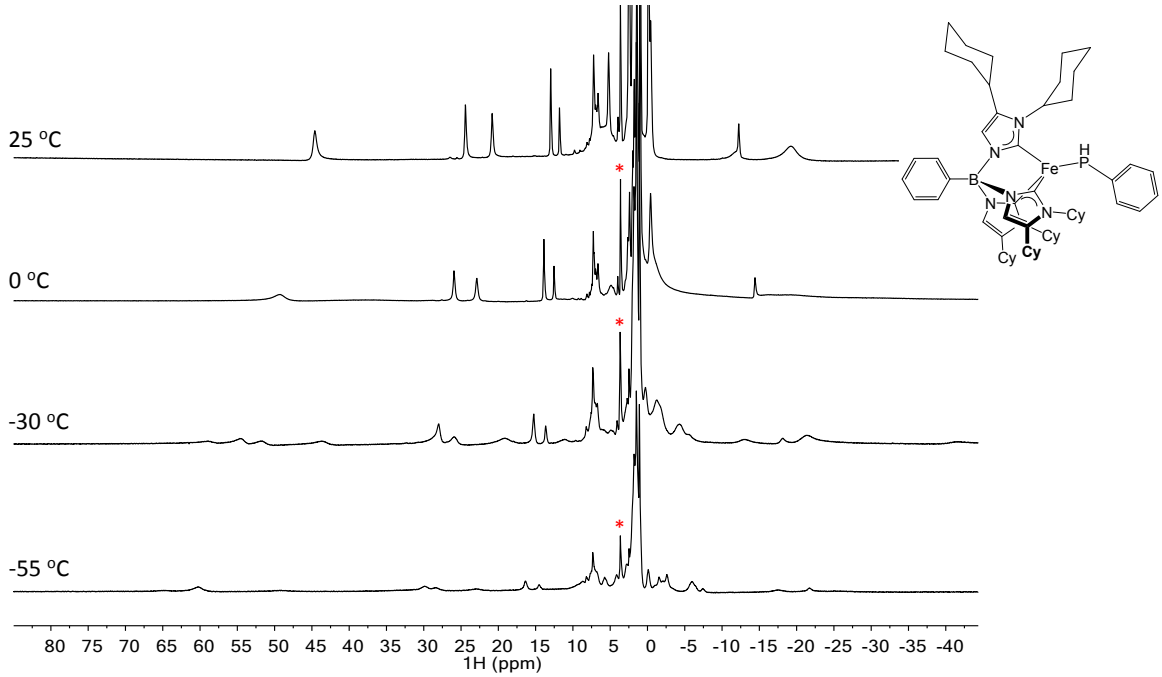

Figure S12. Variable temperature ^{1}H NMR spectra (400 MHz, C_6D_6, 25 °C) of complex $PhB(Cy_2Im)_3$ $Fe(PH(C_6H_5))$(**1b**).

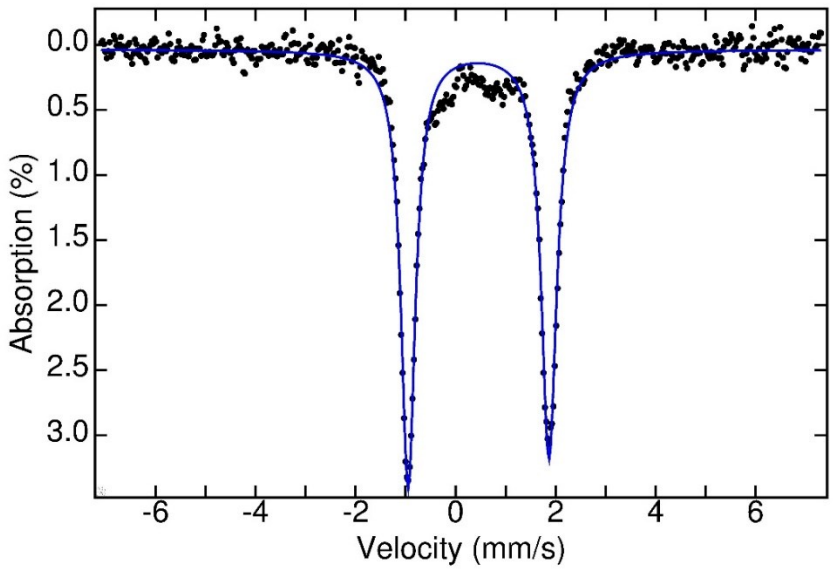

Figure S13. Mössbauer spectrum of complex $PhB(Cy_2Im)_3Fe(PH(C_6H_5))$ **1b** at zero applied field (purple). Parameters for **1b**: δ 0.46 mm/s, ΔE_Q 2.82 mm/s, Γ = 0.37 mm/s. These spectral parameters for **1b** are similar to those of other iron(II) tris(carbene)borate complexes.[7]

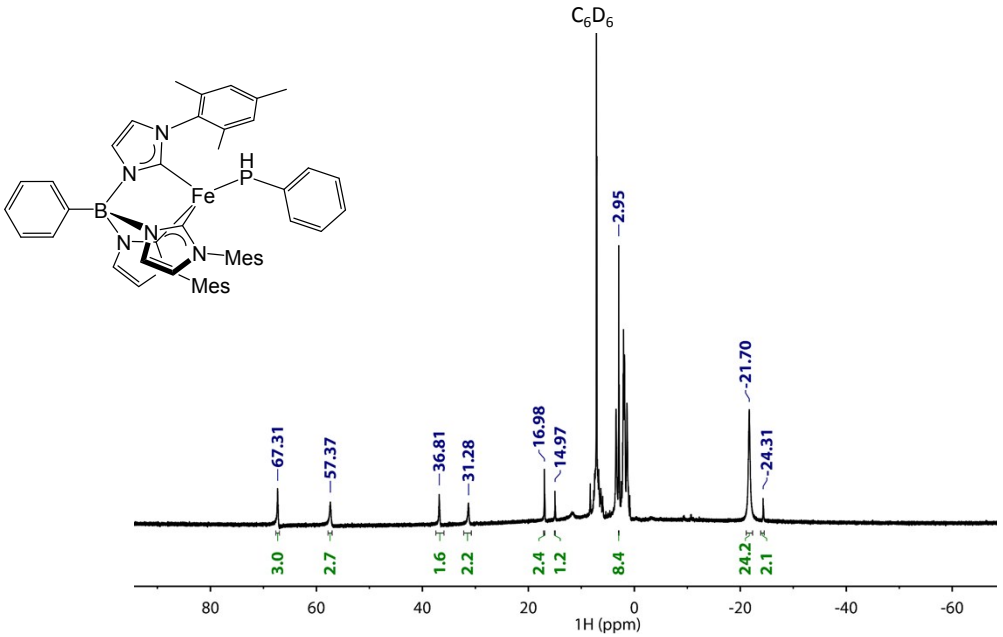

Figure S14. ^1H NMR spectrum (400 MHz, C_6D_6, 25 °C) of complex $PhB(MesIm)_3Fe(PH(C_6H_5))$ (**1c**).

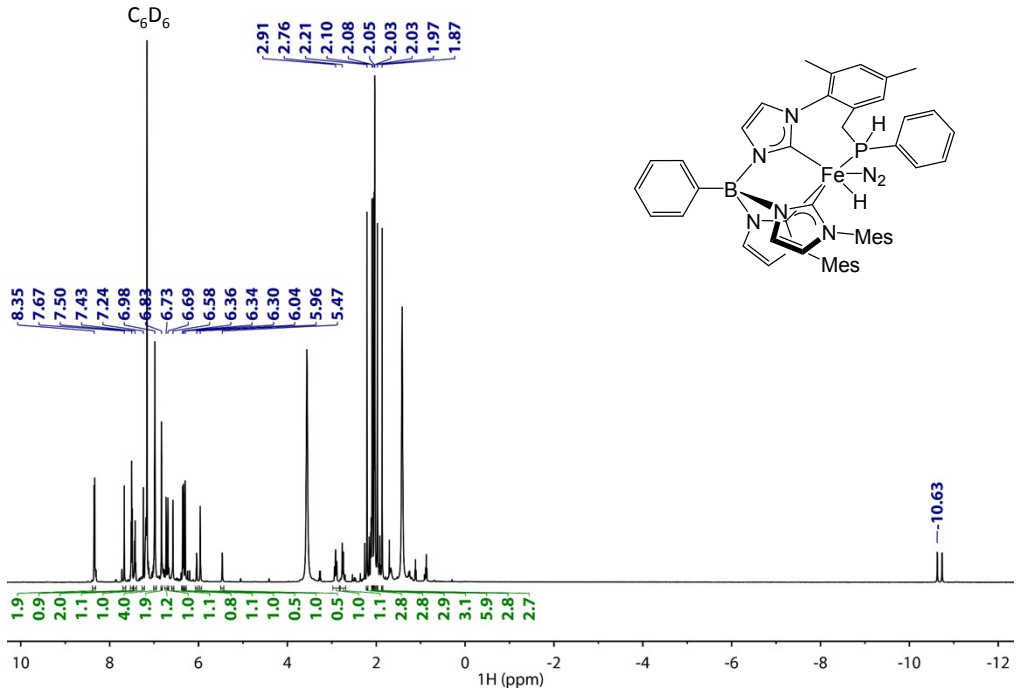

Figure S15. ^{1}H NMR spectrum (500 MHz, C_6D_6, 25 ^{o}C) of complex **2**.

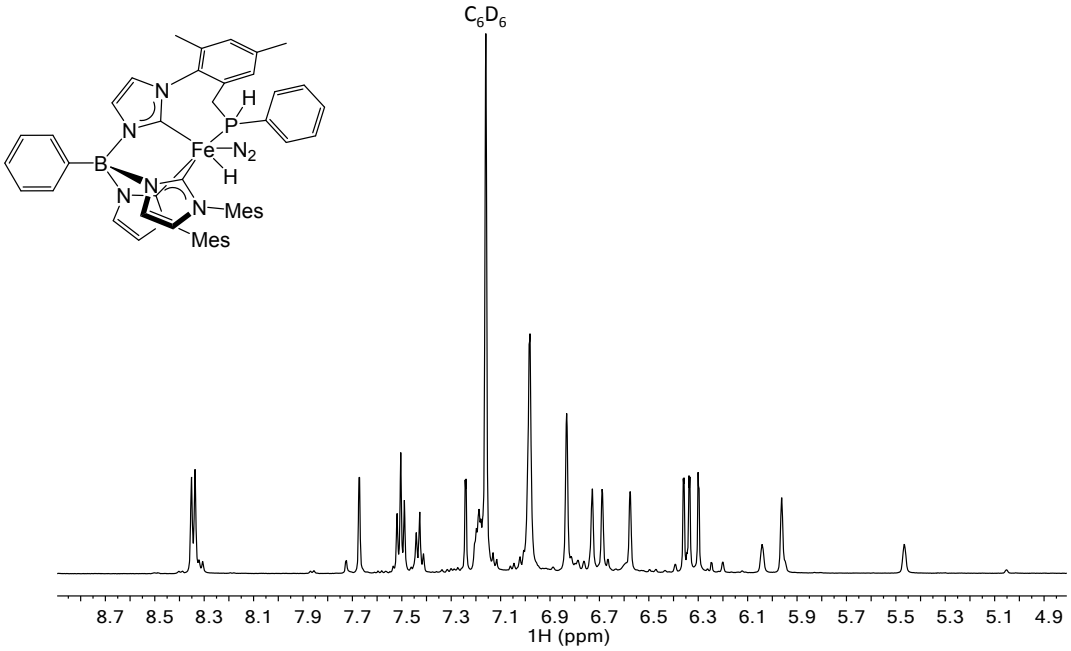

Figure S16. Expansion of the ^{1}H NMR spectrum (500 MHz, C_6D_6, 25 ^{o}C) of complex **2** showing the aromatic resonances. The P*H* proton is shown at 5.75 ppm ($^{1}J_{HP}$ = 285 Hz).

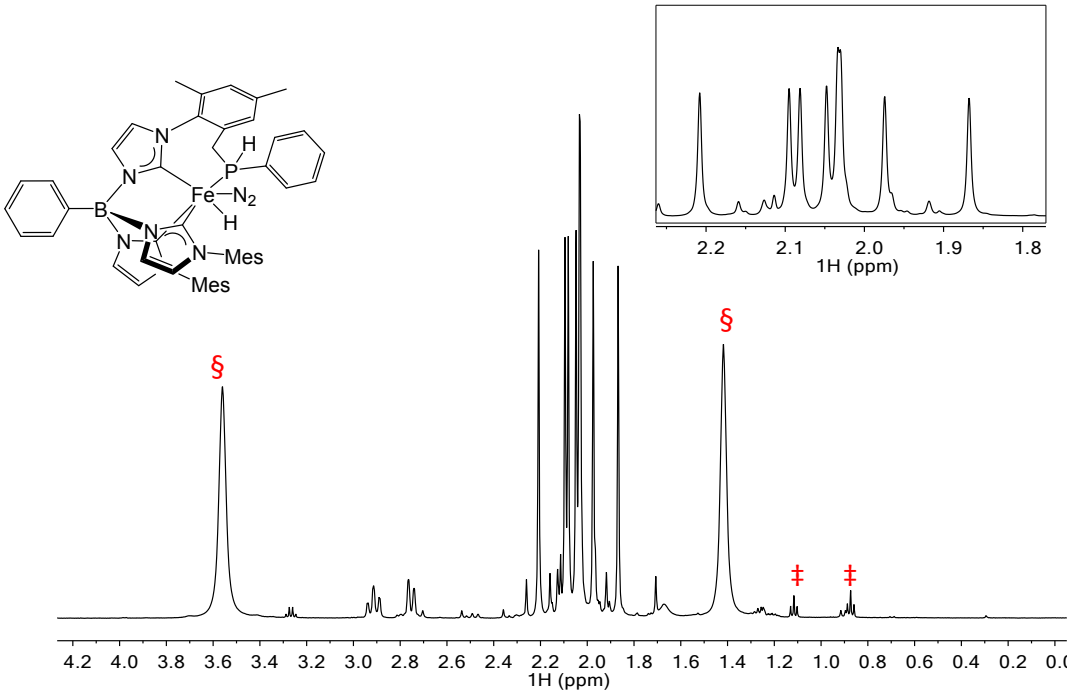

Figure S17. Expansion of the ^{1}H NMR spectrum (500 MHz, C_6D_6, 25 ^{o}C) of complex **2** showing the aliphatic resonances. The asymmetry of the tris(carbene)borate ligand is demonstrated by eight methyl resonances presenting around 2.0 ppm (inset). The symbols (§) and (‡) represent THF from LiPHPh(THF) and pentane, respectively.

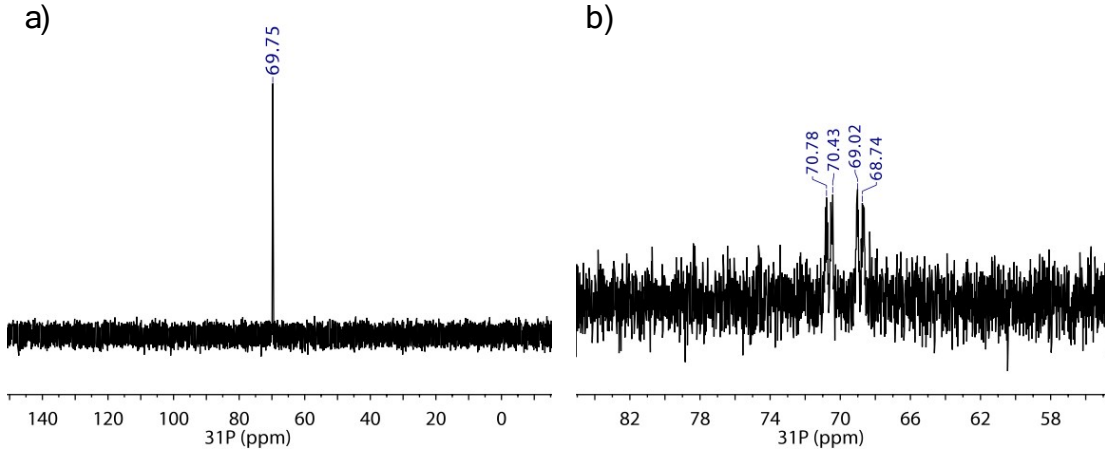

Figure S18. (a) ^{31}P{^{1}H} NMR spectrum (200 MHz, C_6D_6, 25 ^{o}C) and (b) ^{31}P NMR spectrum (162 MHz, C_6D_6, 25 °C) of complex **2**, showing $^{1}J_{HP}$ = 281 Hz and $^{2}J_{HP}$ =57 Hz.

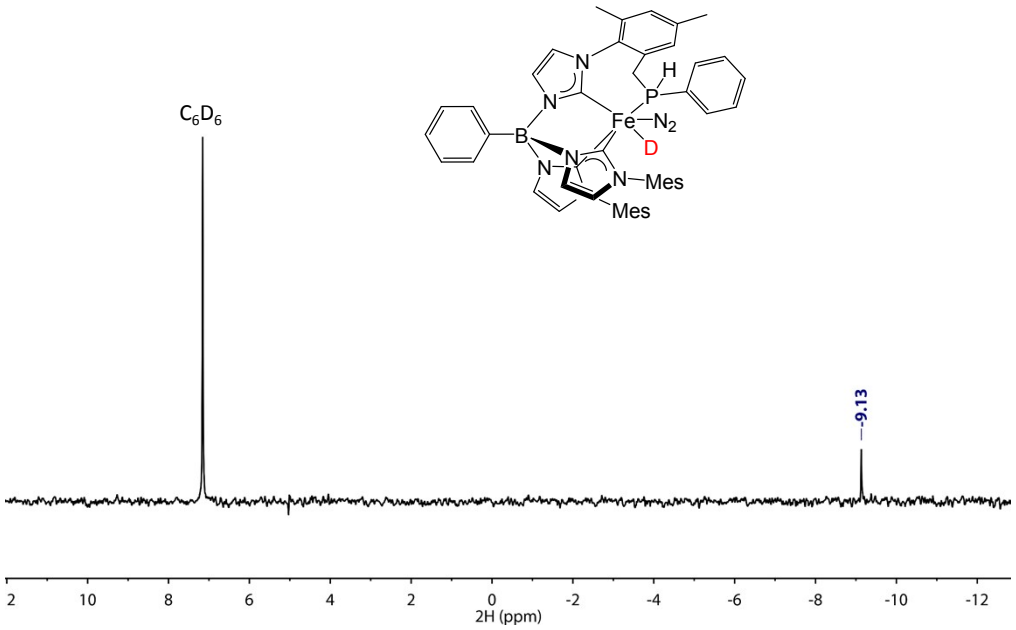

Figure S19. ^{2}H NMR spectrum (61.4 MHz, C_6D_6, 25 ^{o}C) of complex **2-*d***.

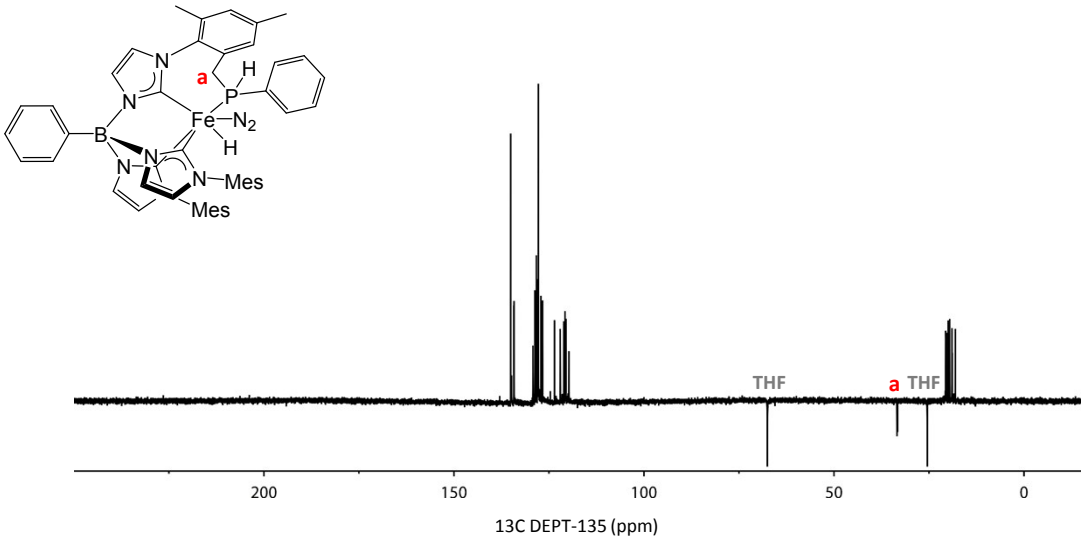

Figure S20. ^{13}C DEPT-135 NMR spectrum (125 MHz, C_6D_6, 25 ^{o}C) of complex **2**. The label **a** indicates the assignment of the phosphino methylene resonance. Free THF is also labeled.

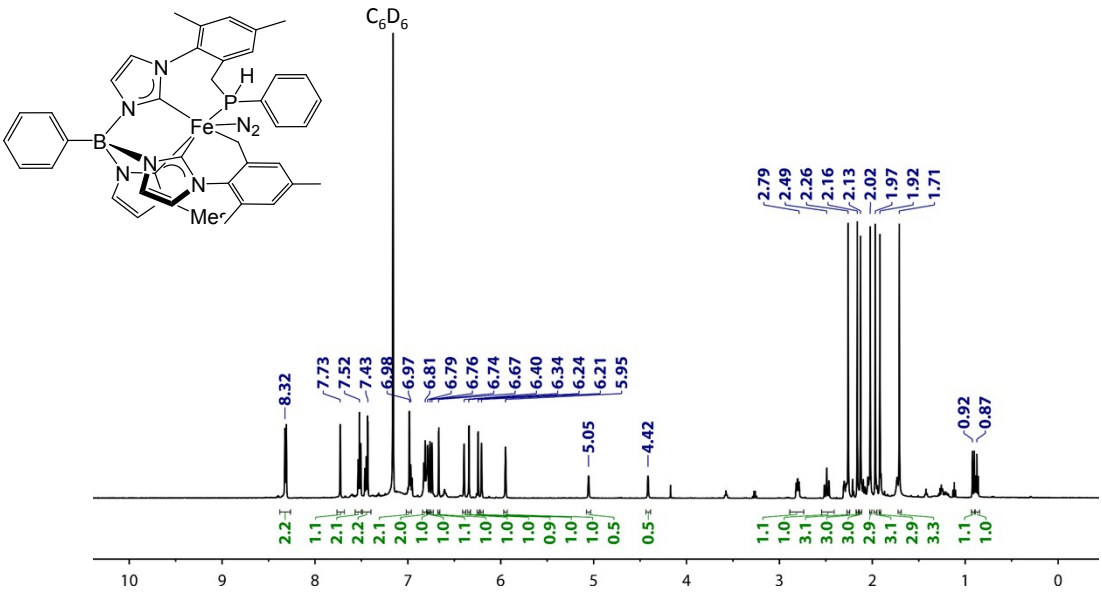

Figure S21. ^{1}H NMR spectrum (500 MHz, C_6D_6, 25 ^{o}C) of complex **3**.

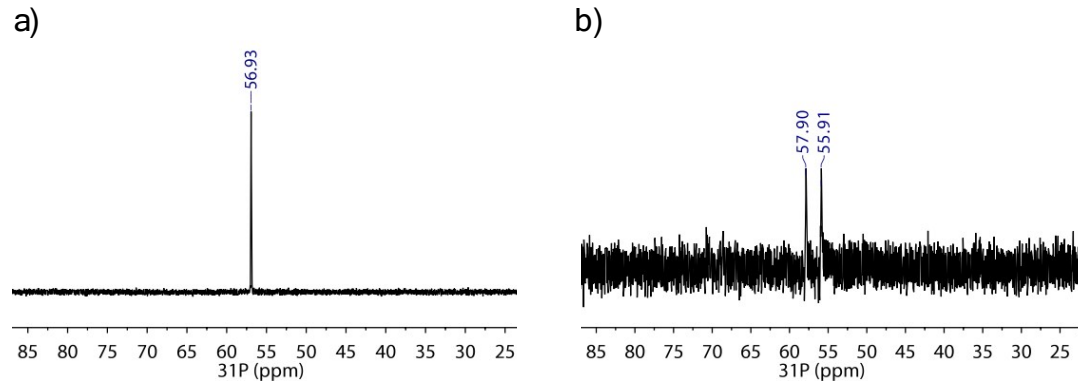

Figure S22. (a) ^{31}P{^{1}H} NMR spectrum (162 MHz, C_6D_6, 25 ^{o}C) and (b) ^{31}P NMR spectrum (162 MHz, C_6D_6, 25 ^{o}C) of complex **3**, showing $^{1}J_{HP}$ = 322 Hz.

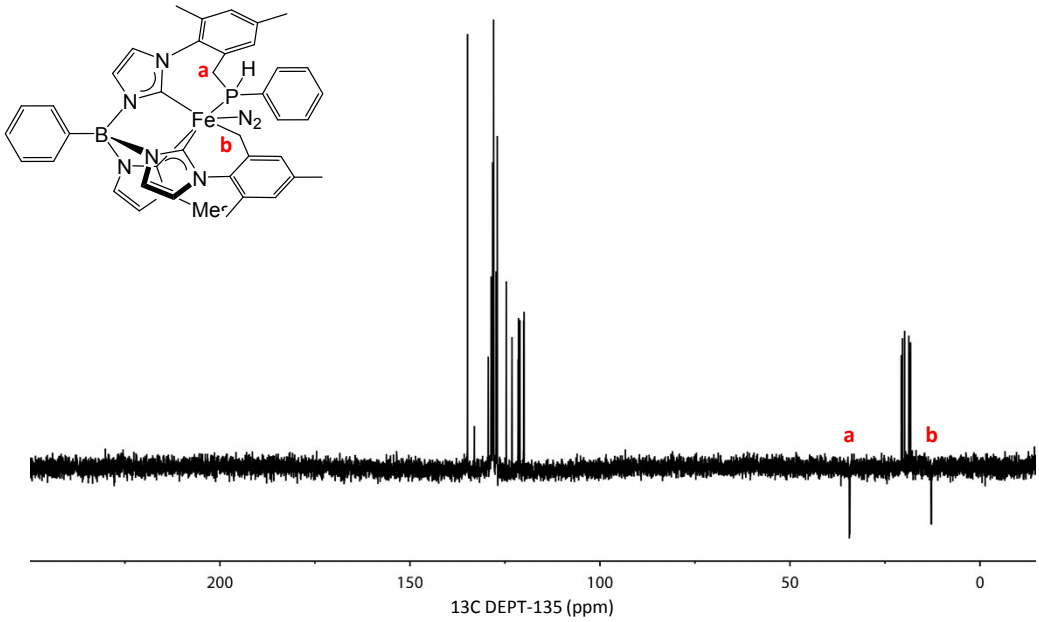

Figure S23. ^{13}C DEPT-135 NMR spectrum (125 MHz, C_6D_6, 25 °C) of complex **3**. The labels **a** and **b** indicate the assignments of the phosphino methylene (**a**) and cyclometalla-methylene (**b**) resonances.

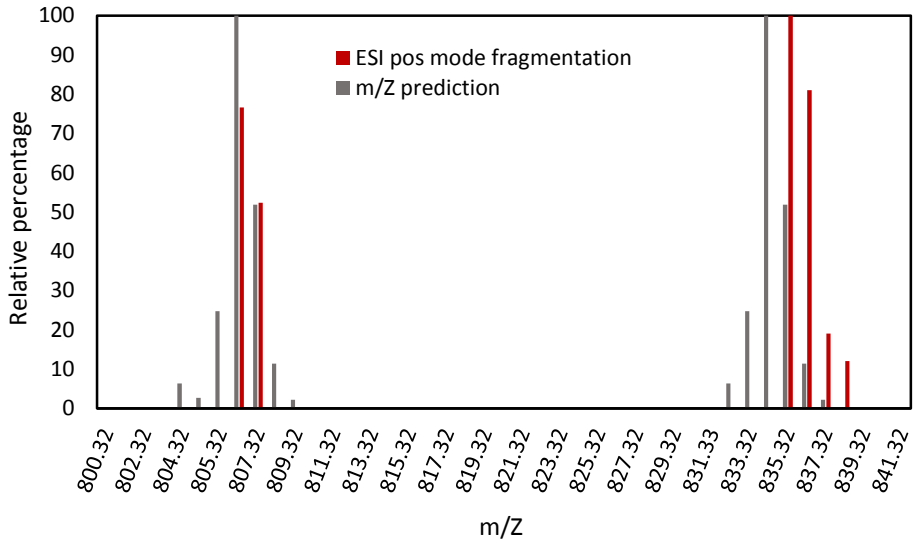

Figure S24. Predicted m/Z fragmentation of complex **3** ($C_{48}H_{48}BFeN_6P$ and $C_{48}H_{48}BFeN_8P$, gray), and experimental ESI-MS (positive mode) of complex **3** (red). ESI-MS: Found 806.3 $\{M^+\}$; $C_{48}H_{48}BFeN_6P$ requires 806.58. Found 835.3 $\{M+H\}^+$; $C_{48}H_{48}BFeN_8P$ requires 834.32.

Kinetics Studies

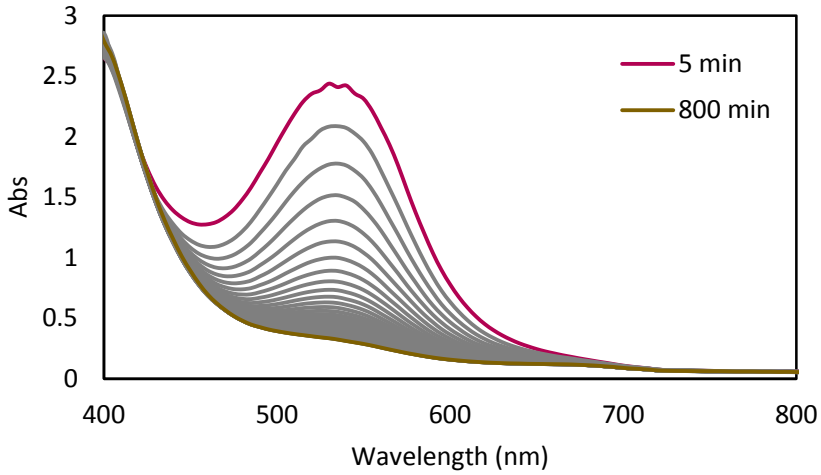

Figure S25. Example plot of the decay of PhB(MesIm)$_3$Fe(PH(C$_6$H$_5$)) (**1c**) over 14 hours. Details: Complex PhB(MesIm)$_3$FeCl (12 mg, 0.016 mmol), and LiPH(C$_6$H$_5$) (5 mg, 0.026 mmol) were dissolved in C$_6$H$_6$ (10 mL) and stirred for 2 minutes. The purple slurry was filtered through Celite and an aliquot was transferred to the quartz cuvette. The reaction was monitored in 20 minutes intervals for 14 hours held at 30 °C.

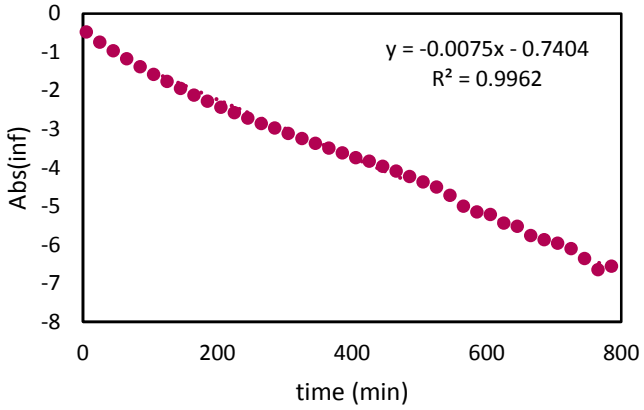

Figure S26. Example plot of first-order fit of the decay of PhB(MesIm)$_3$Fe(PH(C$_6$H$_5$)) (**1c**) over 13 hours at 600 nm. The rate constant k_{obs} is 0.0074(5) min^{-1}, giving a half-life ($t_{1/2}$) of 92 min (1.53 h).

Table S1. Summary of replicates for fit of the decay of PhB(MesIm)$_3$Fe(PH(C$_6$H$_5$)) (**1c**). The average k_{Hobs} is 0.0070(4) min^{-1}.

Run	k_{Hobs} (min^{-1})
1	0.0075(1)
2	0.0064(4)
Average	0.0070(4)

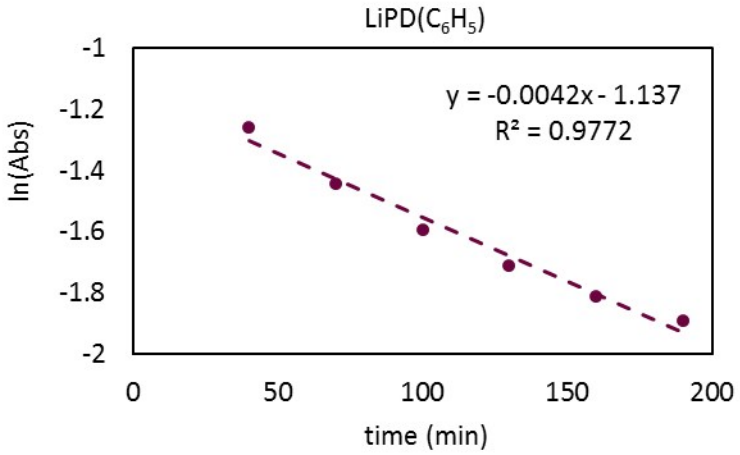

Figure S27. Example plot of first-order fit of the decay of PhB(MesIm)$_3$Fe(PD(C$_6$H$_5$)) (**1c-*d***) over 3 hours at 600 nm. The rate constant k_{obs} is 0.0042(3) min^{-1}, giving a half-life ($t_{1/2}$) of 2.75 h. Details: Complex PhB(MesIm)$_3$FeCl (11 mg, 0.015 mmol), and LiPD(C$_6$H$_5$) (95%, 7 mg, 0.060 mmol) were dissolved in C$_6$H$_6$ (5 mL) and stirred for 6 minutes. The purple slurry was filtered through Celite and an aliquot was transferred to the quartz cuvette. The reaction was monitored in 30 minutes intervals for 20 hours, held at 30 °C.

Table S2. Summary of replicates for fit of the decay of PhB(MesIm)$_3$Fe(PD(C$_6$H$_5$)) (**1c-*d***). The average k_{Dobs} is 0.0049(4) min^{-1}. Using the average k_{Hobs} (Table S1) and k_{Dobs}, the observed KIE is 1.4(2).

Run	k_{Dobs} (min^{-1})
1	0.0042(3)
2	0.0057(3)
Average	0.0049(4)
KIE	1.4(2)

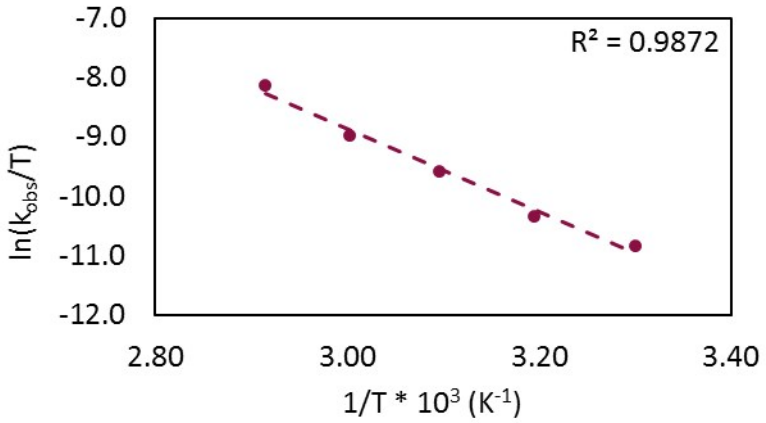

Figure S28. Determination of activation parameters for the decay of PhB(MesIm)$_3$FePH(C$_6$H$_5$) **(1c)**. $\Delta H^{\ddagger}$ = 13.9(9) kcal mol^{-1}, $\Delta S^{\ddagger}$ = -0.020(3) kcal mol^{-1}K^{-1}. Details: For each trial, run in replicate, PhB(MesIm)$_3$FeCl (approx. 8 mg) and LiPH(C$_6$H$_5$) (approx. 6 mg) were stirred in C$_6$H$_6$ (4 mL) for 5 minutes. The slurry was filtered through Celite and an aliquot was transferred to the quartz cuvette. Absorbance measurements were recorded every 5 minutes for 4 h using cycle mode of the data collection software. The decay at 600 nm was plotted as a first order fit to determine k_{obs} at each temperature. Temperatures shown are 30, 40, 50, 60, and 70 °C. The activation barrier ($\Delta G^{\ddagger}$) at 30 °C is 20.9(9) kcal mol^{-1}.

Computational Details

All calculations were performed using density functional theory as implemented in the Orca computational software package.[8] Geometry optimizations for all complexes were performed with the B3LYP functional, Grimme[9] D3 dispersion corrections, and def2-SVP[10] basis sets. Reevaluation of the electronic energies (single point energy corrections) was done with def2-TZVP basis set. Additionally, the Fe center was treated with the DKH2 effective core potential to increase computational efficiency. Vibrational/rotational/translational entropies of the solute(s) were included using standard thermodynamic approximations. Solvation energies were determined by a self-consistent reaction field (SCRF) approach. Solvation calculations were carried out on optimized gas phase geometries employing the dielectric constant of $\varepsilon = 7.25$ (THF). The standard set of optimized radii were used to generate the solute surface. All structures were verified to be minima on the potential energy surface by the removal of imaginary frequencies. Determination of the change in solution phase free energy $\Delta G_{(sol)}$ was calculated as follows:

$$\Delta G_{(sol)} = \Delta G_{(gas)} + \Delta\Delta G_{solv}$$

$$\Delta G_{(gas)} = \Delta H_{(gas)} - T\Delta S_{(gas)}$$

$$\Delta H_{(gas)} = \Delta E_{(scf)} + \Delta ZPE$$

$\Delta G_{(gas)}$ = change in gas phase free energy; $\Delta\Delta G_{solv}$ = change in free energy pf solvation; $\Delta H_{(gas)}$ = change in gas phase enthalpy; T = temperature (298.15 K); $\Delta S_{(gas)}$ = change in gas phase entropy; $\Delta E_{(scf)}$ = self-consistent field energy or the electronic energy at the triple-ζ level; ΔZPE = change in vibrational zero point energy.

Computational Results

Three likely spin states were modeled to locate an intermediate along the reaction pathway. The relative free energies of these complexes are presented in Table S3.

Table S3. Relative energies of the three spin states.

Spin State (*S*)	ΔG_{sol} (kcal/mol)
0	10.01
1	15.46
2	0.00

The geometry optimizations reveal that lowest energy structure is on the $S = 2$ surface (Table S3) and is the four-coordinate iron(II) phosphido complex proposed experimentally. As expected, the structure is similar to that of the crystallographically characterized analogue, **1a**, but with a shorter Fe-P bond length, presumably due to less steric congestion for this tris(carbene)borate ligand.

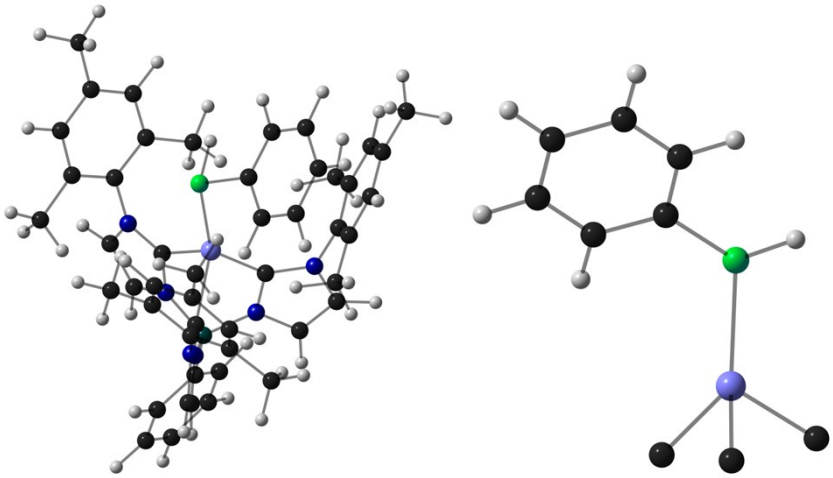

Figure S29. Optimized structure of **1c** (B3LYP-D3/def2-SVP). Selected bond lengths (Å) Fe-P 2.355 Å, Fe-C_{Im}(avg) 2.078 Å.

Interestingly, geometry optimization on the $S = 0$ surface converges to a different structure in which a hydride ligand bridges a Fe-P bond. Optimization of a phophinidene hydride structure also converges to this geometry. The Fe-P bond is 2.067 Å, indicative of multiple bond character. This structure is expected to be thermally accessible.

Orbital analysis reveals that the phosphorus 3p orbital makes a large contribution to the HOMO. Mullikan orbital analysis show that the HOMO has 32.8 % phosphorus character, this is indicative of a nucleophilic phosphorus and provides a mechanism for the observed C-H insertion reactivity. Furthermore, the percent orbital character on the phosphorus increases from the starting complex **1c** which has less than 10 % phosphorus p character in all four SOMOs shown in Figure S30 below.

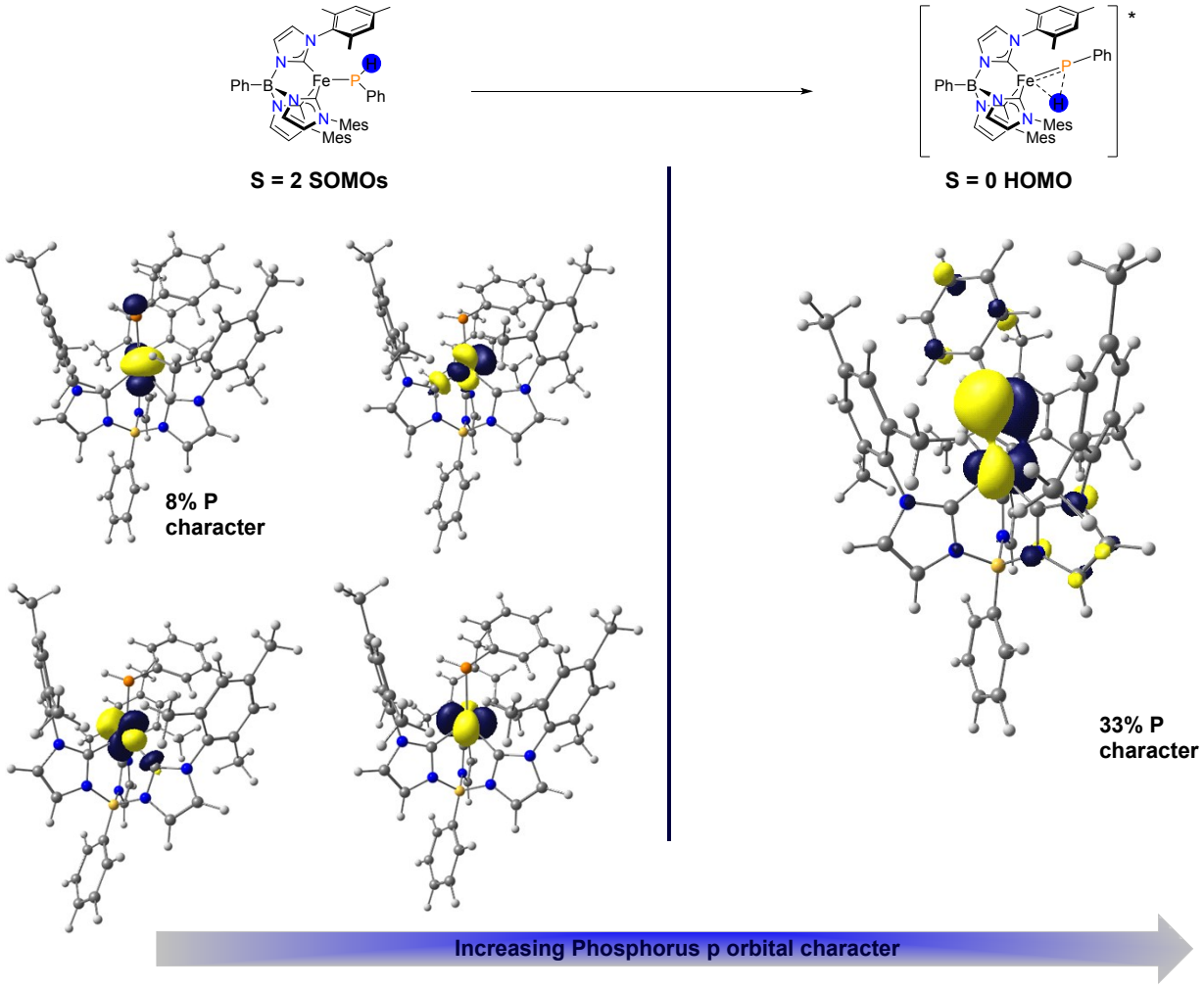

Figure S30. Visualized frontier molecular orbitals for **1a** and the proposed $S = 0$ intermediate. The high spin SOMOs very visualized by a corresponding orbital transformation (COT)[11] that matches the occupied α and β orbitals according to their best spatial overlap.

Additional orbital analysis into the proposed $S = 0$ intermediate shows a delocalized 3-center-2-electon orbital between the Fe-P-H unit at HOMO – 24. The orbital consists of 12.1 % Fe, 5.9 % H, and 8.4 % P character.

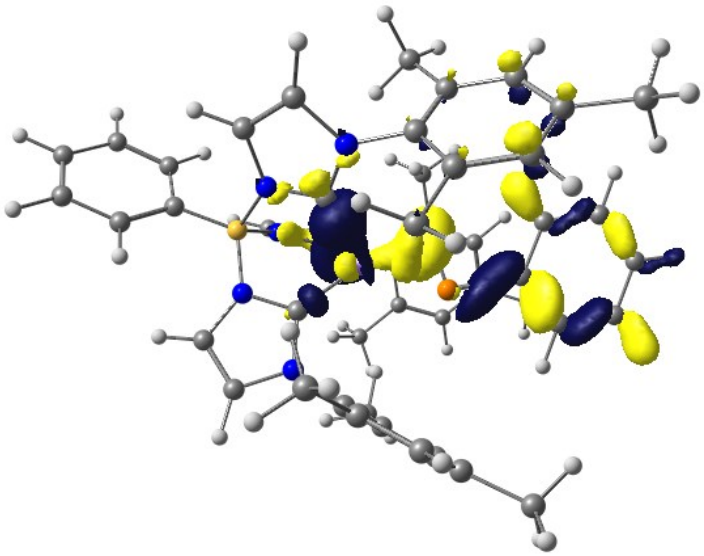

Figure S31. 3-center-2-electron orbital (HOMO – 24) in the proposed $S = 0$ intermediate.

The triplet, which is slightly higher in energy than the $S = 0$ intermediate, also has a structure with a bridging hydride about the Fe-P bond similar to the $S = 0$ species. However, orbital analysis shows that the SOMOs are solely metal based and show no nucleophilic phosphorus character shown in Figure S32 below.

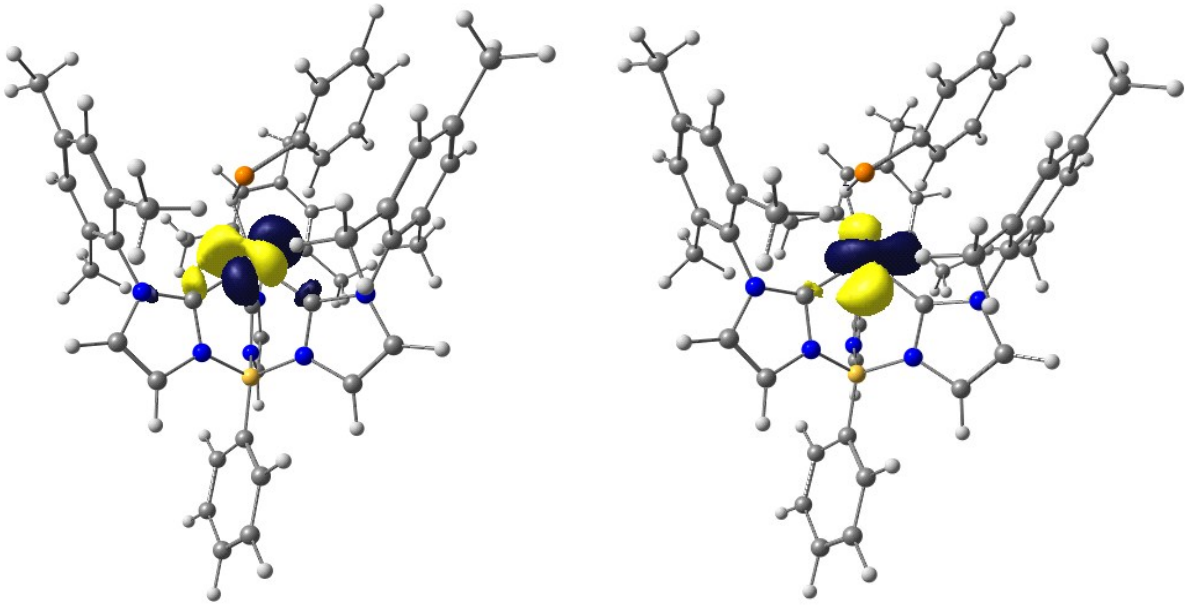

Figure S32. $S = 1$ SOMOs after a COT show no phosphorus orbital character.

To estimate the energy of an iron phosphinidene hydride complex ([Fe](H)(=PPh)), a linear synchronous transit (LST) calculation was performed on a model complex, in which the Fe-P bond distance was systematically shortened from that of the optimized $S = 0$ geometry (Figure S33). The optimized $S = 0$ state is found to be 2 kcal/mol higher in energy than the $S = 2$ state, suggesting that steric interactions in the real complex disfavor formation of the arrested α-hydride migration structure.

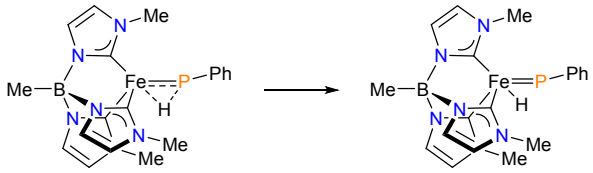

Figure S33. LST calculation in a model complex for the conversion of the arrested iron(II) α-hydride complex to an iron(IV) phosphinidene hydride.

The results of these calculations demonstrate that formation of a phosphinidene is energetically unfavorable. Specifically, even the formation of a long Fe-H bond (1.6 Å) in a phosphinidene species is at least 50 kcal/mol uphill from the optimized structure (Table S4, Figure S34). (Note that the optimal Fe=P bond distance in an iron(II) phosphinidene complex is experimentally unknown). This energy difference is expected to be even larger for the full complex, where steric interactions between the phosphido and tris(carbene)borate ligand substituents will occur. Thus, formation of a transient phosphinidene that inserts into the C-H is unlikely.

Table S4. Results of the LST calculation for a model complex (Figure S33). Energies are relative to the optimized structure of the arrested iron(II) α-hydride structure.

Fe-P (Å)	Fe-H (Å)	P-H (Å)	E(kcal/mol)
1.6	1.588727	1.66565	80.7611
1.634481	1.598055	1.654084	64.85371
1.668961	1.609883	1.636489	51.61025
1.703442	1.624332	1.618932	40.51592
1.737923	1.640223	1.604044	31.29441
1.772404	1.656566	1.590068	23.66272
1.806884	1.674672	1.576912	17.49603
1.841365	1.689837	1.565996	12.30028
1.875845	1.705229	1.556809	8.340643
1.910327	1.72799	1.545826	5.376457
1.944807	1.751953	1.536432	3.215848
1.979287	1.773555	1.528767	1.663973
2.013768	1.793292	1.522596	0.638554
2.04825	1.814945	1.517202	0.137136
2.08273	1.836246	1.511737	0

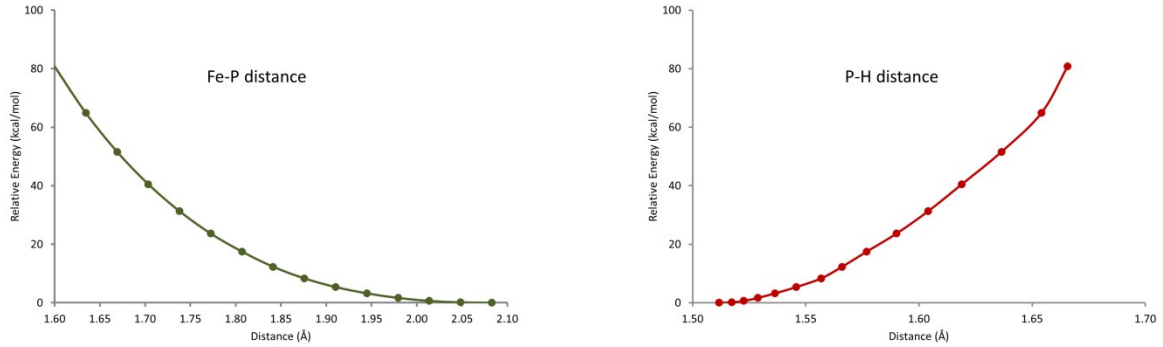

Figure S34. Plots of energy vs Fe-P (left) and P-H (right) distances from the LST calculation.

In order to investigate the steric impact of the hydride transfer to the Fe center, geometry optimizations for the $S = 2$ reactant and the proposed $S = 0$ intermediate were done on the tert-butyl tris(carbene)borate derivative, **1a**. The calculated free energies to form the $S = 0$ intermediate are presented below (Table S5) and compared to the mesityl analogue (**1c**).

Table S5: Calculated free energy from the $S = 2$ reactant to the proposed $S = 0$ intermediate for different N-alkylated NHC substituents. Energies are in kcal/mol.

R-group	S = 2 (kcal/mol)	S = 0 (kcal/mol)
^{t}Bu	0.00	29.7
Mes	0.00	10.1

The DFT calculations suggest that the steric profile of the *N*-substituted imidazolylidene donors greatly affects the bridged hydride formation. The sterically bulky *tert*-butyl groups are less accommodating towards the phosphorus ligands moving closer to the Fe center, whereas the planar mesityl groups allow for more facile access to the Fe center. Thus, **1c** has more favorable thermodynamics for the formation of the $S = 0$ proposed intermediate. The calculated thermodynamics for the $S = 0$ complex formation for **1a** is much too high to be reasonably accessible under reaction conditions.

Crystallographic Information

Data collection

The data collection was carried out using Mo Kα radiation (graphite monochromator) with a selected frame time and detector distance. A randomly oriented region of reciprocal space was surveyed to achieve complete data with a redundancy of 4. Sections of frames were collected with 0.50º steps in ω and ϕ scans. Data to a resolution of 0.86 Å were considered in the reduction. Final cell constants were calculated from the xyz centroids of strong reflections from the actual data collection after integration (SAINT).[12] The intensity data were corrected for absorption (SADABS).[13]

Structure solution and refinement

The space groups were determined based on intensity statistics and systematic absences. The structure was solved using SIR-92[14] and refined (full-matrix-least squares) using the Oxford University Crystals for Windows system.[15] A direct-methods or intrinsic methods solution was calculated, which provided most non-hydrogen atoms from the E-map. Full-matrix least squares/difference Fourier cycles were performed, which located the remaining non-hydrogen atoms. All non-hydrogen atoms were refined with anisotropic displacement parameters. The hydrogen atoms were placed in ideal positions and refined as riding atoms.

PhB(^{t}BuIm)$_3$Fe(PH(C_6H_5)) (Complex 1a)

Empirical formula	C34.68 H48.19 B Fe N6 O0.42 P	
Formula weight	653.43	
Crystal color, shape, size	red block, 0.35 × 0.30 × 0.22 mm^3	
Temperature	150(2) K	
Wavelength	0.71073 Å	
Crystal system, space group	Monoclinic, C2/c	
Unit cell dimensions	a = 37.4525(14) Å	α = 90°.
	b = 16.3865(6) Å	β = 90.917(2)°.
	c = 11.1300(4) Å	γ = 90°.
Volume	6829.8(4) Å^3	
Z	8	
Density (calculated)	1.271 Mg/m^3	
Absorption coefficient	0.523 mm^{-1}	
F(000)	2781	
Data collection		
Diffractometer	APEX II Kappa Duo, Bruker	
Theta range for data collection	1.09 to 30.12°.	
Index ranges	-50<=h<=52, -23<=k<=23, -15<=l<=15	
Reflections collected	72837	
Independent reflections	10042 [R(int) = 0.0374]	

Observed Reflections	8224
Completeness to theta = 30.12°	99.8 %
Solution and Refinement	
Absorption correction	Semi-empirical from equivalents
Max. and min. transmission	0.8936 and 0.8381
Solution	Intrinsic methods
Refinement method	Full-matrix least-squares on F^2
Weighting scheme	$w = [\sigma^2 Fo^2 + AP^2 + BP]^{-1}$, with
	$P = (Fo^2 + 2\,Fc^2)/3$, A = 0.0585, B = 23.8040
Data / restraints / parameters	10042 / 3 / 393
Goodness-of-fit on F^2	1.058
Final R indices [I>2sigma(I)]	R1 = 0.0576, wR2 = 0.1469
R indices (all data)	R1 = 0.0701, wR2 = 0.1558
Largest diff. peak and hole	1.000 and -0.930 e.Å^{-3}

$PhB(Cy_2Im)_3FeCl$

Empirical formula	C55 H84 B Cl Fe N6 O
Formula weight	947.39
Crystal color, shape, size	colorless block, 0.21 × 0.21 × 0.11 mm^3
Temperature	150(2) K
Wavelength	0.71073 Å
Crystal system, space group	Monoclinic, $P2_1/n$
Unit cell dimensions	a = 11.3237(19) Å α = 90°.
	b = 25.174(4) Å β = 104.370(9)°.
	c = 19.208(3) Å γ = 90°.
Volume	5304.1(15) Å^3
Z	4
Density (calculated)	1.186 Mg/m^3
Absorption coefficient	0.378 mm^{-1}
F(000)	2048
Data collection	
Diffractometer	APEX II Kappa Duo, Bruker
Theta range for data collection	1.36 to 27.31°.
Index ranges	-14<=h<=13, 0<=k<=32, 0<=l<=24
Reflections collected	26753
Independent reflections	11589 [R(int) = 0.0495]
Observed Reflections	7880
Completeness to theta = 27.31°	96.8 %
Solution and Refinement	
Absorption correction	Semi-empirical from equivalents
Max. and min. transmission	0.9596 and 0.9245

Solution	Intrinsic methods
Refinement method	Full-matrix least-squares on F^2
Weighting scheme	$w = [\sigma^2 Fo^2 + AP^2]^{-1}$, with $P = (Fo^2 + 2\,Fc^2)/3$, A = 0.707
Data / restraints / parameters	11589 / 32 / 604
Goodness-of-fit on F^2	1.044
Final R indices [I>2sigma(I)]	R1 = 0.0513, wR2 = 0.1215
R indices (all data)	R1 = 0.0882, wR2 = 0.1320
Largest diff. peak and hole	0.435 and -0.436 e.Å^{-3}

$PhB(Cy_2Im)_3Fe(PH(C_6H_5))$ (Complex 1b)

Empirical formula	C58.25 H82.50 B1 Fe1 N6 P1	
Formula weight	964.47	
Crystal color, shape, size	red block, 0.05 × 0.20 × 0.20 mm^3	
Temperature	150(2) K	
Wavelength	0.71073 Å	
Crystal system, space group	Monoclinic, $P2_1/n$	
Unit cell dimensions	a = 10.5900(4) Å	α = 90°.
	b = 26.1279(9) Å	β = 91.277(2)°
	c = 40.2762(14) Å	γ = 90°.
Volume	11141.4(4) Å^3	
Z	8	
Density (calculated)	1.150 Mg/m^3	
Absorption coefficient	0.341 mm^{-1}	
F(000)	4160	
Data collection		
Diffractometer	APEX II Kappa Duo, Bruker	
Theta range for data collection	1.011 to 25.051°.	
Index ranges	-12<=h<=11, -27<=k<=31, -47<=l<=46	
Reflections collected	65100	
Independent reflections	19582 [R(int) = 0.0374]	
Observed Reflections	19673	
Completeness to theta = 30.12°	99.7%	
Solution and Refinement		
Absorption correction	Semi-empirical from equivalents	
Max. and min. transmission	0.8936 and 0.8381	
Solution	Intrinsic methods	
Refinement method	Full-matrix least-squares on F^2	
Weighting scheme	$w = [\sigma^2 Fo^2 + AP^2 + BP]^{-1}$, with $P = (Fo^2 + 2\,Fc^2)/3$, A = 0.0585, B = 23.8040	
Data / restraints / parameters	19582 / 131 / 1217	
Goodness-of-fit on F^2	0.9403	

Final R indices [I>2sigma(I)]	R1 = 0.0915, wR2 = 0.2092
R indices (all data)	R1 = 0.1793, wR2 = 0.2441
Largest diff. peak and hole	1.96 and -1.53 e.Å^{-3}

Complex 2

Empirical formula	C54.25 H65 B Fe N8 P
Formula weight	926.77
Crystal color, shape, size	yellow block, 0.18 x 0.17 x 0.11 mm^3
Temperature	150(2) K
Wavelength	0.71073 Å
Crystal system, space group	Monoclinic, $P2_1/n$
Unit cell dimensions	a = 16.1882(6) Å α = 90°.
	b = 21.3706(8) Å β = 100.3102(18)°.
	c = 29.4853(10) Å γ = 90°.
Volume	10035.8(6) Å^3
Z	8
Density (calculated)	1.227 Mg/m^3
Absorption coefficient	0.377 mm^{-1}
F(000)	3940
Data collection	
Diffractometer	APEX II Kappa Duo, Bruker
Theta range for data collection	1.18 to 27.56°.
Index ranges	-21<=h<=20, -27<=k<=27, -38<=l<=38
Reflections collected	180301
Independent reflections	23099 [R(int) = 0.0534]
Observed Reflections	17731
Completeness to theta = 27.56°	99.6 %
Solution and Refinement	
Absorption correction	Semi-empirical from equivalents
Max. and min. transmission	0.9597 and 0.9353
Solution	Intrinsic methods
Refinement method	Full-matrix least-squares on F^2
Weighting scheme	$w = [\sigma^2 Fo^2 + AP^2 + BP]^{-1}$, with
	$P = (Fo^2 + 2\,Fc^2)/3$, A = 0.0505, B = 6.6989
Data / restraints / parameters	23099 / 241 / 1260
Goodness-of-fit on F^2	1.012
Final R indices [I>2sigma(I)]	R1 = 0.0419, wR2 = 0.1030
R indices (all data)	R1 = 0.0620, wR2 = 0.1142
Largest diff. peak and hole	0.510 and -0.408 e.Å^{-3}

Complex 3

Empirical formula	C48 H48 B1 Fe1 N8 P1	
Formula weight	834.59	
Crystal color, shape, size	yellow block, 0.030 x 0.022 x 0.020 mm^3	
Temperature	100 K	
Wavelength	0.41328 Å	
Crystal system, space group	Triclinic, P-1	
Unit cell dimensions	a = 12.2416(5) Å	α = 106.3844(10)°.
	b = 12.4664(5) Å	β = 90.0628(11)°.
	c = 13.9258(6) Å	γ = 91.3197(10)°.
Volume	2038.29(15) $Å^3$	
Z	2	
Density (calculated)	1.360 Mg/m^3	
Absorption coefficient	0.456 mm^{-1}	
F(000)	876	
Data collection		
Diffractometer	Bruker Apex Kappa Duo, Bruker	
Theta range for data collection	0.990 to 16.929°.	
Index ranges	-17<=h<=17, -17<=k<=16, 0<=l<=19	
Reflections collected	11548	
Independent reflections	11548 [R(int) = 0.111]	
Observed Reflections	7464	
Completeness to theta = 12.697°	97.0 %	
Solution and Refinement		
Absorption correction	Semi-empirical from equivalents	
Max. and min. transmission	0.99 and 0.99	
Solution	Direct methods	
Refinement method	Full-matrix least-squares on F2	
Weighting scheme	$w = [\sigma^2 Fo^2 + AP^2 + BP]^{-1}$, with	
	$P = (Fo^2 + 2\,Fc^2)/3$, A = 0.036, B = 3.350	
Data / restraints / parameters	11517 / 0 / 535	
Goodness-of-fit on F^2	1.1659	
Final R indices [I>2sigma(I)]	R1 = 0.0622, wR2 = 0.1361	
R indices (all data)	R1 = 0.1122, wR2 = 0.1774	
Largest diff. peak and hole	1.32 and -1.39 $e.Å^{-3}$	

References

1. Nieto, I.; Ding, F.; Bontchev, R.P.; Wang, H.; Smith, J.M. *J. Am. Chem. Soc*. **2008**, *130*, 2716-2717.

2. Scepaniak, J. J.; Fulton, M. D.; Bontchev, R. P.; Duesler, E. N.; Kirk, M. L.; Smith, J. M. *J. Am. Chem. Soc*. **2008**, *130*, 10515.

3. Traylor, T. G.; Tsuchiya, S.; Campbell, D.; Mitchell, M.; Stynes, D.; Koga, N. *J. Am. Chem. Soc.* **1985**, *107*, 604-614.

4. Hou, Z.; Breen, T. L.; Stephan, D. W. *Organometallics* **1993**, *12*, 3158-3167.

5. Baker, M.V.; Field, L.D.; Hambley, T.W. *Inorg. Chem.*, **1988**, *27*, 2872.

6. Ion Prisecaru, WMOSS4 Mössbauer Spectral Analysis Software, www.wmoss.org, 2009-2016.

7. Scepaniak, J.J.; Harris, T.D.; Vogel, C.S.; Sutter, J.; Meyer, K.; Smith, J.M. *J. Am. Chem. Soc.* **2011**, *133*, 3824.

8. Neese, F. *WIREs Comput. Mol. Sci.* **2012**, *2*, 73.

9. (a) Grimme, S.; Ehrlich, S.; Goerigk, L. *J. Comput Chem,* **2011**, *32*, 1456; (b) Grimme, S.; Antony, J.; Ehrlich, S.; Krieg, H. *J. Chem. Phys.* **2010**, *132*, 154104

10. Pantazis, D. A.; Chen, X. Y; Landis, C. R.; Neese, F. *J. Chem. Theory Comput.* **2008**, *4*, 908.

11. Neese, F.J. *Phys. Chem. Solids* **2004**, *65*, 781.

12. SAINT, Bruker Analytical X-Ray Systems, Madison, WI, current version.

13. An empirical correction for absorption anisotropy, R. Blessing, *Acta Cryst*. **1995**, *A51*, 33-38.

14. Altomare, A; Cascarano, G; Giacovazzo, G.; Guagliardi, A.; Burla, M. C.; Polidori, G.; Camalli, M. *J. Appl. Cryst.* **1994**, *27*, 435.

15. Betteridge, P. W.; Carruthers, J. R.; Cooper, R. I.; Prout, K.; Watkin, D. J. *J. Appl. Cryst*. **2003**, *36*, 1487.